Ocean Wave Integral Parameter Measurements Using ENVISAT ASAR Wave Mode Data

X.-M. Li [(1)], S. Lehner [(1)] and Th. Bruns [(2)]

[(1)] German Aerospace Center (DLR), Oberpfaffenhofen, 82234 Wessling, Germany

[(2)] Deutscher Wetterdienst Zentrale (DWD), Frankfurter Straße 135, 63067 Offenbach, Germany

Abstract

An empirical algorithm to retrieve integral ocean wave parameters such as significant wave height (SWH), mean wave period and H_{12} wave height from synthetic aperture radar (SAR) images over the sea surface designed for ENVISAT ASAR wave mode data is presented in this paper. The algorithm based on the CWAVE approach was first developed for ERS-2 SAR wave mode data and is therefore referenced here as CWAVE_ENV. It has the calibrated ASAR wave mode images as the only input and does not need any first guess information from an ocean wave model, which makes the SAR to be an independent instrument measuring integrated wave parameters to Altimeter quality. A globally distributed dataset of 25,000 pairs of ASAR wave mode images and collocated the European Centre for Medium-Range Weather Forecast (ECMWF) reanalysis model results is used for CWAVE_ENV model parameters tuning. Validation carried out by comparing the SWH derived from CWAVE_ENV algorithm to *in situ* buoy measurements shows the scatter index is 24% and comparing to ECMWF model and German Weather Service (DWD) model is 16% and 18% respectively. Two case studies are particularly presented to evaluate the performance of CWAVE_ENV algorithm for high sea state. A North Atlantic storm during which SWH above 18 meters occurred is analyzed was observed by SAR and Radar Altimeter (RA) in synergy. In the Indian Ocean extreme swell case, the potential of ASAR wave mode with CWAVE_ENV algorithm used a forecast tool is demonstrated.

1. Introduction

Ocean waves are the ocean's most obvious surface feature, which interact with atmosphere, ocean currents, bottom topography and with one another. For many reasons, an understanding of their statistical properties is required, such as marine transportation, global climate wave change statistics, as well as ocean wave parameters in specific locations for harbor and ocean engineering, ship design and coastal protection.

Ocean waves are traditionally measured *in situ* at one point, as by moored buoys, which are normally located near to the coast giving very limited spatial coverage. Satellite remote sensing, particularly active microwave sensors, e.g., SAR, offer alternate approaches to observe ocean surface waves on a global scale. As a unique sensor for ocean surface wave measurements, SAR is the only spaceborne sensor that can provide ocean surface images with high resolution, independent of cloud cover and light conditions. In particular, the SAR yields information on the two dimensional spectrum of the sea surface.

The L-band SAR sensor onboard SEASAT launched in 1978 provided a first realization of global ocean surface measurements from space (e.g., see [*Beal et al*, 1983]). From 1991 till now, ERS-1, ERS-2 and ENVISAT missions launched by European Space Agency (ESA) have operationally provided continuous SAR ocean wave measurements. In this paper following an introduction, the current algorithms to derive the two-dimensional ocean wave spectra are briefly summarized.

1.1 Ocean wave measurements from SAR

Nonlinear retrieval approach

The retrieval of ocean wave spectra from SAR image spectra is not a straightforward mapping. The SAR imaging mechanism is nonlinear, because of distortion induced by the wave motions [*Hasselmann et al.*, 1985]. This leads, among other effects, to image smearing and to a loss of information beyond the so-called azimuth cut-off wavelength [*Alpers and Brüning*, 1986]. For ERS and ENVISAT SAR, this corresponds typically to wavelengths shorter than about 100 - 200 m in the satellite flight direction. In addition, ocean wave spectra from satellite SAR images suffer from a basic 180^o ambiguity of wave traveling direction, which can be resolved from the complex data through [*Engen and Johnson*, 1995]. A nonlinear mapping of ocean wave spectra into SAR image spectra as well as its inversion was developed in Max-Planck-Institute for Meteorology by 0 referred to as MPI Scheme in the following**.** This inversion algorithm enables a reliable retrieval of ocean wave spectra from SAR spectra within the computational constraints of real-time operational applications (see also [*Krogstad*, 1992] for the simpler transform). An assessment of the performance of the retrieval algorithm as well as the operational feasibility was given by [*Heimbach et al.*, 1998] using three years (1993-1995) of ERS-1/SAR wave mode UWA spectra data [*Brooker*, 1995]. Validation results show that approximately 75% of the available SAR wave mode spectra data yielded successful retrievals. There is a small overestimation less than 0.5 m of retrieved significant wave height (SWH) by MPI scheme compared to WAM model [*WAMDI GROUP*, 1998].

A semi-parametric algorithm was developed as well for full ocean wave spectrum retrieval from SAR by taking the ERS/SAR wave mode spectra and collocated ERS wind scatterometer wind vectors into account as additional input [*Mastenbroed and de Valk*, 1998]. The algorithm becomes could not be used for the ENVISAT mission on which the scatterometer is not onboard.

A retrieval scheme for the derivation of two-dimensional ocean wave spectra from look cross spectra provided by the ENVISAT ASAR operating in wave mode [ENVISAT Handbook] is presented by [*Schulz-Stellenfleth et al.*, 2005, referred to as PARSA algorithm] which needs a prior information from numerical wave model as well [ESA Report].

SAR cross spectral algorithm

Using two looks of SAR wave mode complex data, the cross spectral algorithm can be derived to remove the 180º ambiguity of ocean wave propagation direction and reduce the speckle noise significantly, e.g., described by [*Lehner et al.*, 2000].

Demonstrated on airborne C-band SAR data, the cross spectral algorithm was developed to retrieve two-dimensional ocean wave spectra [*Engen and Johnson*, 1995], which is adopted by ESA for the ASAR wave mode data of the ENVISAT mission as called WVW level2 products. The retrieved ocean wave spectra of the Level2 products only yield information on longer wave [*Abadalla et al.*, 2008] contained in the ASAR wave mode data due to the cut-off effect of SAR ocean wave imaging mechanism.

To some extent, the PASAR algorithm introduced above is the combination of the nonlinear approach and cross spectral algorithm. It uses the cross spectrum of two looks to remove 180º ambiguity and blend the SAR image spectra and first prior information from wave model to solve the nonlinear effect of SAR ocean wave imaging process.

Empirical algorithm

For the current non-linear or quasi-linear algorithms retrieving 2D ocean wave spectra from SAR imagery either first prior information from numerical wave model (e.g., MPI scheme or PARSA scheme) is needed or only a limited part of the spectra for waves longer than a certain threshold, e.g., ESA Level2 products algorithm, can be derived.

A new approach using an empirical algorithm is given to derive ocean wave integral parameters, e.g., SWH or mean wave period, rather than 2D spectra, which does not need prior information. For the ERS mission, the empirical algorithm of CWAVE_ERS [*Schulz-Stellenfleth et al.*, 2007] to derive integral wave parameters was developed for reprocessed ERS-2 SAR wave mode data [*Lehner et al.*, 2000]. Validation results show that the performance of CWAVE _ERS is fairly good when compared to the ECMWF WAM model using 6000 collocation data pairs and to 21 buoy measurements from a time frame of three weeks. For SWH comparisons, both have quite small bias and RMS of 0.44 m and 0.39 m, respectively.

1.2 New empirical algorithm CWAVE_ENV

More than 17 years SAR global ocean observation data have been acquired since the launch of ERS-1 in 1991. Another independent active satellite measurement of SWH thus becomes available contributing to global wave climate analysis in addition to the altimeter data. It is possible using as well ENVISAT ASAR data to develop an algorithm to derive integrated wave parameters without any prior information leading to a homogenous ocean surface wave measurements for nearly 20 years SAR wave mode dataset.

In this study, a new empirical algorithm to derive integral wave parameters from ENVISAT ASAR wave mode data is developed, which is referred to as CWAVE_ENV. CWAVE_ENV empirical model function is adopted from the CWAVE_ERS algorithm developed for ERS-2 SAR reprocessed wave mode data. Considering ASAR wave mode data have different spatial resolutions, image size, calibration constant and ocean surface imaging performance with ERS-2 SAR wave mode data, new tuned coefficients for CWAVE_ENV model is a bit more demanding. Using the CWAVE_ENV model, a global dataset of ocean wave integral parameters from ENVISAT ASAR wave mode data independent of any prior information becomes available.

The paper is organized as follows. In section 2, the dataset used in this study is introduced in more detail. The empirical model approach and validation are demonstrated in section 3. Global sea state statistics derived from ASAR wave mode data acquired in December 2006, January and February 2007 are compiled in chapter 4. Two case studies, a North Atlantic storm generating wind seas with SWH above 18 meters and a high ocean swell above 7 meters in Indian Ocean are presented in section 5. Finally, summary and conclusions are given.

2. Description of Data Sources

2.1 ENVISAT ASAR Wave Mode Data

When ASAR is operated in the wave mode, a small are image covering 6 km x 5 km to 10 km x 5 km, namely referred to as imagettes are acquired along the orbit every 100 km. Compared to ERS/SAR wave mode data, acquisition of ENVISAT ASAR wave mode is much more flexible. It is operated in C-band with multiple incidence angles from 15º~45.2º, namely IS1~IS7, as well two single polarizations, i.e., VV and HH. ASAR wave mode data yield a resolution of 4 m in azimuth direction and 20 m in range direction.

In the present study, the following filters are implemented for the ASAR wave mode data used in CWAVE_ENV model for tuning and validation.

(1) Only the ASAR wave mode data acquired in IS2 swath with incidence angles at around 23º and VV polarization are used.

(2) To avoid effects of sea ice in the North and South Polar, only the wave mode data acquired between -70º S~70º N are included in the dataset.

(3) Homogeneity test is performed on the ASAR wave mode data. Examples of homogenous ASAR wave mode data and inhomogeneous one are given in Figure1 (a) and (b) respectively. The ratio of image variance and squared image mean is set to 1.05 as a threshold to classify the ASAR wave mode imagettes into classes of homogenous or inhomogeneous cases [*Schulz-Stellenfleth and Lehner*, 2004]. Around 9% ASAR imagettes acquired in 2006 December fail to pass the homogeneity test, and they are excluded from the CWAVE_ENV model parameters tuning and validation dataset.

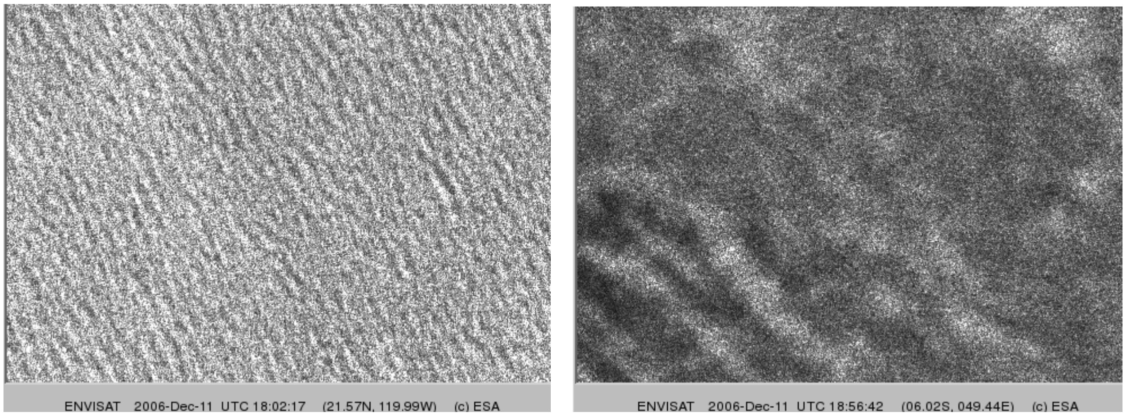

(a) (b)

Figure 1. *Examples of ENVISAT ASAR wave mode data acquired over sea surface for homogenous case (a) and inhomogeneous one (b)*

2.2 Numerical Wave Model Data

Summary of the third generation WAve Model (WAM) is given in the report of the WAMDI Group [1984]. From June 1992 a new version of WAM called cycle 40 was introduced operationally at the ECMWF. For global ocean forecast, the horizontal resolution of WAM operated in ECMWF can reach 1.5 º, and for regional forecast a higher resolution model up to 10 km can be provided, e.g., the WAM version operated in DWD.

The WAM model is expressed in terms of an action balance equation:

$$\frac{\partial E}{\partial t} + C_g \frac{\partial E}{\partial x} = S = S_{in} + S_{nl} + S_{ds} \qquad (1)$$

where:

$E = E(f, \theta, x, t)$ is the two-dimensional wave spectrum depending on frequency f, and direction of propagation θ, time *t* with different locations of *x*.

C_g is the deep-water group velocity;

S is the net source function, consisting of three terms;

S_{in}: Energy input by wind;

S_{nl} :Non-linear energy transfer by wave-wave interactions;

S_{ds} : Dissipation.

The ocean wave integral parameters SWH and mean wave period (zero upcrossing period used in this study) can be derived from model one dimensional spectra as given in (2) and (3).

$$H_s = 4\sqrt{\int E(f,\theta)df\,d\theta} \qquad (2)$$

$$T_{m02} = \sqrt{\int E(f,\theta)dfd\theta \Big/ \int E(f,\theta)\,f^2 dfd\theta} \qquad (3)$$

Modelers have contributed continues effort to improve the wave model forecast performance. During 1992-1993 in ECMWF, mean RMSE of the 24 hours forecast SWH was around 0.75m. A significant improvement was achieved in 2002-2003 decreasing the mean RMSE to around 0.25 m, in which the contribution of large increase observation of sea state and surface wind provided by satellites, e.g., RA, SAR and Scatterometer, is notably [*Janssen*, 2008]. Some high resolution local numerical wave models have improved their abilities to analyze extreme sea state. For instance the LSM (Local Sea wave Model) operated in DWD was compared to two selected severe winter storms in North Atlantic and shows high quality for short-period forecast [*Behrens and Günther*, 2008]. However, with respect to long term global wave model performance assessment, there is still room for improvement as shown in the ERA-40 wave products validation. SWH shows slight overestimation (<1.5 m) in low sea state and substantially underestimation by more than 20% in high sea state when compared to the RA of Topex and in situ buoy measurements [*Caires and Sterl*, 2003].

In this paper, WAM 2D spectra collocated with the ASAR imagettes are provided by ECMWF as collected from the CERSAT collocation system [CERSAT-Ifremer]. These WAM spectra are achieved at 6-hour interval (at 00, 06, 12 and 18 UTC). Therefore, the time of the ASAR imagettes are matched with that of spectra within ± 3 hours. The grid spacing for the location of ASAR imagettes and the nearest WAM model grid point is 0.5 degree. The

WAM 2D spectra are provided on a polar grid with 24 direction bins and 30 frequency bins beginning from 0.03452Hz with a logarithmic increment of 1.1Hz. One should point out, that the collocated WAM model has been assimilated ASAR wave mode cross spectra information, referred to as the ECMWF reanalysis model in the following.

Integral ocean wave parameters on grid points are provided by the DWD for this study instead of 2D spectra. Spatial and temporal resolution of the model is 0.75º and 3 hours, respectively. Validation of SWH derived from the DWD 24-hour forecast GSM model shows a good agreement with a positive bias of 0.04 m and scatter index of 20.2% when compared to buoy measurements during June to August 2007 [*Bidlot et al*., 2007].

2.3 Buoy Data

To validate the CWAVE_ENV empirical model, buoy data collected from the CERSAT collocation system are used. Figure 2 shows a map of 77 buoys used for the validation. Most of the buoys are from the NOAA National Data Buoy Center (NDBC) and the Environment Canada Marine Environmental Data Service (MEDS).

The non-directional buoys are used to measure the sea surface vertical acceleration, which can be used to derive surface displacement spectra. The details of the data collection and analysis procedures for the NDBC non-directional wave buoys were described in detail by [*Steele and Earle*, 1979]. Generally, in each hour a 20-minute record of vertical hull accelerations of the buoy, sampled at a rate of 1Hz, is collected. By doing a segmented FFT for the record, an acceleration spectrum is calculated and the non-directional wave spectrum $S(f)$, i.e., frequency spectrum, is obtained from it.

Integrated wave parameter e.g., SWH can be estimated from the frequency spectrum $S(f)$ of the wave displacement record according to following equation, see as well formula (2), using a limitation of frequencies in addition:

$$Hs = 4\left[\int_{f_0}^{f_1} S(f)df\right]^{1/2} \quad (4)$$

The frequencies usually range from 0.03 to 0.40 Hz at intervals of 0.01 Hz.

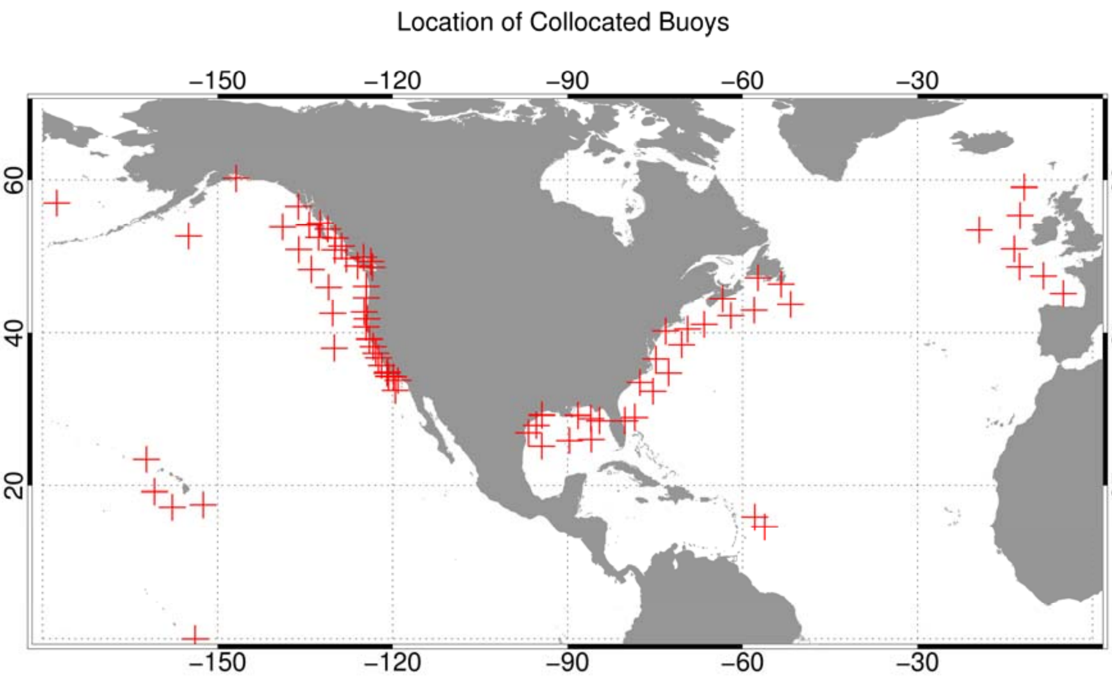

Figure 2. Location of collocated buoys used for CWAVE_ENV model validation

The name, latitude and longitude information of the buoy stations as shown in Figure 2 are given in Appendix A.

3 CWAVE_ENV Model Tuning Approach

In this section, the CWAVE_ENV parametric model structure, model fitting procedure and its evaluation using the tuning dataset are described in detail.

3.1. Introduction of the Parametric Model

3.1.1. Multiple Regression Model

Suppose n parameters or factors $S(s_{1,\dots,n})$ are thought to affect the expected observation W with coefficients $A(a_{1,\dots,n})$. A simple linear regression model collecting these parameters to be used an estimator is expressed by (5) see [*von Storch and Zwiers*, 1999],

$$W = a_0 + \sum_{i=1}^{N} a_i s_i + E_i \qquad (5)$$

where E_i are random variables with zero mean. Formula (5) is the simple linear regression for modeling *n* data points and independent factors, which corresponds to a straight line. For the CWAVE_ENV empirical model, a quadratic term is added on the right side of formula (5), i.e., it is a multiple linear model, taking account into the nonlinearities as well as possible coupling among different variables. Thus the final form of the model is given as,

$$W = a_0 + \sum_{i=1}^{N} a_i s_i + \sum_{i=1}^{N} \sum_{j=1}^{i} a_{i,j} s_i s_j \qquad (6)$$

The model states that the observation *W* is expressed as a linear combinations of the factors $S(s_{1,\ldots,n})$ and thus the model is linear in its parameters. However, the factors themselves can be nonlinear functions of other variables. In following the variables chosen in CWAVE_ENV model are introduced.

3.1.2. ASAR Image Parameter Selection in the CWAVE_ENV Model

Using model given by the formula (6) it is assumed that the *n* variables include all relevant predictor variables. It is often required to select the variables such that no essential information is lost. On the other hand, too many variables will increase the computational consuming as well as make the model rather sensitive to minor changes.

In the CWAVE_ENV model, we assume that ASAR parameters S_A ($s_{1,\ldots,}s_n$), i.e. Normalized Radar Cross Section (NRCS, referred as well $\sigma_\circ$ as shown in formula (7)), variance of the normalized SAR image (*cvar*, see formula (8) [*Kerbaol*, 1998]), and other parameters computed from variance spectrum can be regarded as related to ocean surface wave. Previous research described that due to the cut off effect of SAR imaging mechanism only longer wave information is contained in the spectrum, particularly apparent for high altitude orbit SAR system, e.g., ERS SAR and ENVISAT ASAR. At the same time, NRCS of SAR image is related to ocean surface wind based on the CMOD function [*Stoffelen and Anderson*, 1997; *Lehner et al.*, 1998] and thus can represent short wave information.

$$\sigma_0 = 10 * \log_{10}\langle I \rangle - K \tag{7}$$

$$c\,\text{var} = \frac{I - \langle I \rangle}{\langle I \rangle} \tag{8}$$

In (7) and (8), $\langle I \rangle$ is the mean intensity of ASAR wave mode data and K is the calibration constant.

Estimation of the ASAR image spectrum is performed by computing the image periodogram with two-dimensional FFT algorithm. The raw periodogram is not a good spectral estimation because of spectral bias and the fact that the variance at a given frequency does not decrease as the number of samples used in the computation increases. The variance problem can be reduced by smoothing the periodogram, i.e., the so-called method of averaged periodogram. The idea behind it is to divide the entire set with N samples into many sub sets with M samples, compute the FFT of each sub set, square it to get the power spectral density and compute the average of the ensemble. This approach implemented on the ASAR image spectral estimation is given in Appendix B.

In the both models of CWAVE_ERS and CWAVE_ENV, 20 parameters are extracted from the estimated two-dimensional SAR image spectra. Together with $\sigma_{\circ}$ and *cvar*, there are 22 parameters that are collected into the ASAR image parameter vector S ($s_{1,\ldots,}s_n$) as input to model (6).

Although the exact physical meaning behind (6) is not easily to be interpreted, the 22 parameters derived from the ASAR image include essential information relating the image itself to both long wave and short wave information therefore the parametric model is successful in estimating ocean wave integral parameters.

3.2. Empirical Model Fitting Procedure

A least square minimization approach is used to tune the CWAVE_ENV empirical model as given by (9), where *W* is the integral wave parameter (e.g., SWH or mean wave period) derived from model or other observation data sources collocated to ASAR image and treated as the “true” ,or at least very reliable sea state observations. It needs to be pointed out that different integrated wave parameter corresponds to respective parametric model coefficients.

$$J_{\cos t}(A) = \sum_{j=1}^{N} (W^{(j)} - \sum_{i=1}^{k} A_i S_i^{\,j})^2 \tag{9}$$

As stepwise regression procedure is used for the least square minimization approach. The 22 parameters defined in the previous section are all included in the tuning approach; however there are possibilities that some parameters will not lead to a significant improvement of the empirical model. To diagnose the performance of every SAR image parameters collected in vector S_A ($s_{1,\ldots,}s_n$), couples of terms are used to quantify it.

The sum of squares due to regression denoted SSR

$$SSR = \sum_{j=1}^{N} (W - \sum_{i=0}^{k} A_i S_i^{\,j}) \tag{10}$$

The sum of squared errors $SS\varepsilon$ is

$$SS\varepsilon = \sum_{j=1}^{N} (W_j - \sum_{i=0}^{k} A_i S_i^{\,j}) \tag{11}$$

The multiple-regression is performed on every ASAR image parameter. The parameter S_i for which SSR_1 is largest is chosen as the initial parameter. In the next step, a new parameter S_{i+1} is selected, for which the incremental regression sum of squares SSR_{inc} is again largest.

$$SSR_{inc} = SSR_{i+1} - SSR_i \tag{12}$$

In the third step, the testing of hypothesis that the inclusion of new ASAR parameter S_{i+1} significantly reduces the regression sum of squares are performed by computing the test variable of,

$$F^{(i+1)} = \frac{SSR_{inc}}{SS\varepsilon_{i+1}/(N-i)} \quad (13)$$

This is compared to the critical value of the distribution $F(1, N-i)$ [*von Storch and Zwiers*, 1999], if the testing variable $F^{(i+1)}$ is below 0.99 or 99% quantiles the iteration to select ASAR parameters will be terminated and the coefficients in (6) are fitted. Otherwise the parameter S_{i+1} will be excluded from the model and the steps are repeated till the testing variable satisfies the critical value.

3.2. CWAVE_ENV Model Implementation

In the CWAVE_ENV empirical model, 22 parameters as introduced in the previous sector extracted from ASAR wave mode image are used for parametric model tuning approach.

In the present study, ASAR collocated ECMWF spectra from December 2006 are used as the tuning dataset.

Histograms of SWH and Tm_{02} derived from these collocated reanalysis ECMWF model spectra are shown in Figure 3(a) and (b), respectively. It can be observed that the tuning dataset includes different sea state and the dominant SWH ranges between 1.5 m ~ 2.5 m contributing around 50% to the entire tuning dataset. The maximum SWH measured by the ECMWF model in the tuning dataset is 12.6 m. The Tm_{02} distribution shows that the model measures numerous waves with period between 8 s ~ 9 s and long swell with periods larger than 12 s does exist in the tuning dataset, too.

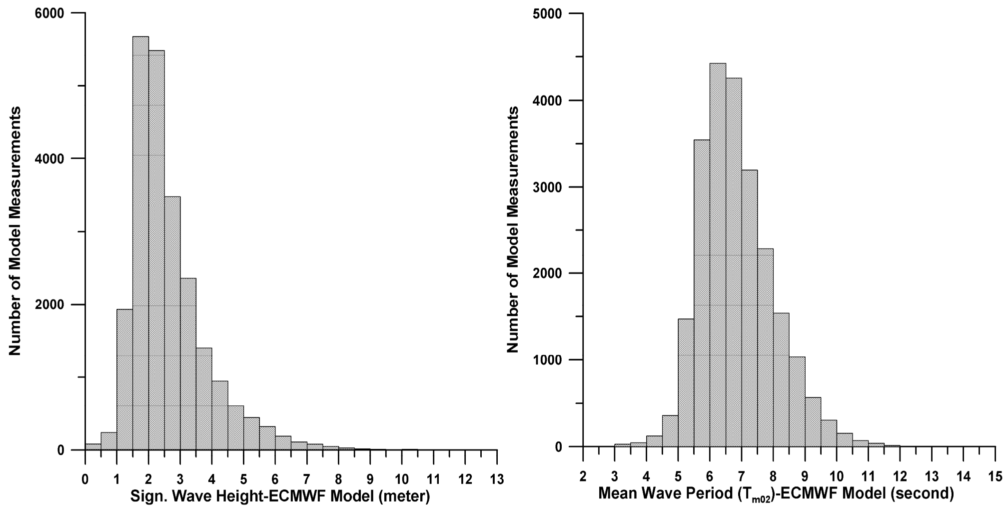

(a) (b)

Figure 3. Histogram of SWH (a) and T_{m02} (b)) used in tuning dataset of CWAVE_ENV model which are derived from ECMWF analyzed model in 2006 December

The tuning dataset is used for the CWAVE_ENV model parameter fitting approach. Figure 4 shows the comparison results for SWH (left panel) and T_{m02} of the tuning dataset to the ECMWF reanalysis model results. The differences between ASAR measurements Y_i and observations X_i (numerical model or buoy) are quantified in terms of bias, root-mean-square-square (RMSE) and scatter index (SI), which are expressed in the form of (14), (15) and (16), respectively.

$$Bias = \overline{Y_i} - \overline{X_i} \tag{14}$$

$$RMSE = \sqrt{\frac{\sum (Y_i - X_i)^2}{n}} \tag{15}$$

$$SI = \frac{1}{\overline{X_i}} \sqrt{\frac{1}{n} \sum \left[\left(Y_i - \overline{Y_i}\right) - \left(X_i - \overline{X_i}\right)\right]^2} \tag{16}$$

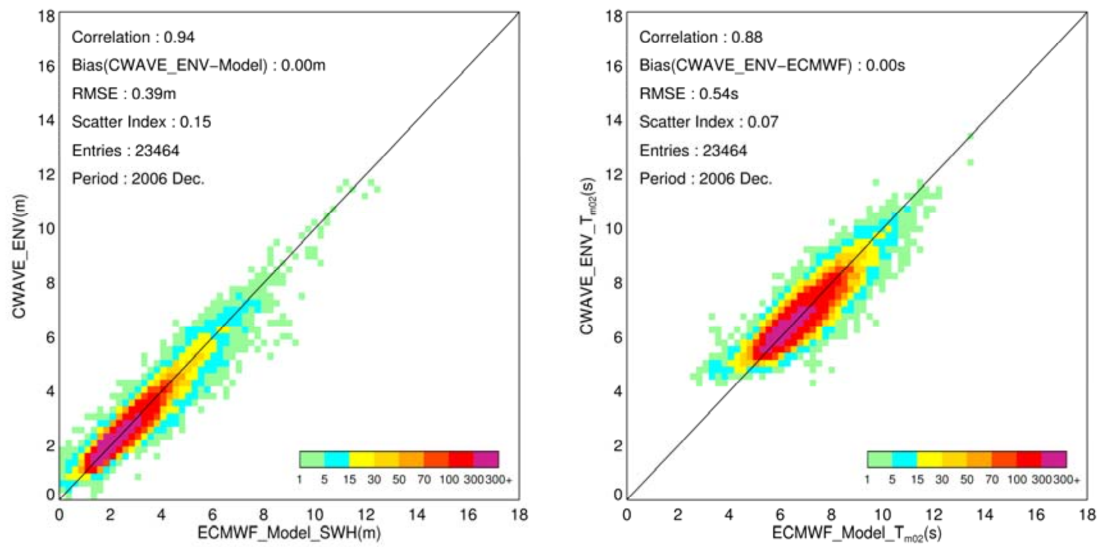

Figure 4. Evaluation for the tuning datasets of CWAVE_ENV model

One can see that the tuning approach of the CWAVE_ENV empirical model is successful making the difference between ASAR measurements derived by the CWAVE_ENV algorithm and the ECMWF reanalysis model results in the tuning dataset quite small with zero bias as to be expected for the tuning, and low scatter indices of 15% and 7% for SWH and T_{m02} respectively.

4. Assessment of the CWAVE_ENV Empirical Algorithm Performance

In this section, SWH, T_{m02} and H_{12} derived from ASAR wave mode data are validated with in situ and numerical wave model comparisons.

Wave height H_{12} (for waves with period larger than 12 seconds) as given by (17) is associated with wave components with wave length longer than 220 m. Such waves are directly detectable as patterns on the ASAR images. On the other hand, validation results show that SWH derived from numerical wave models, e.g., WAM operated in ECMWF there is a large positive bias (larger than 0.25 m) related to swell events (e.g., wave period in the range of 10-15s) generated by storms in the Southern Hemisphere winter time when compared to *in situ* buoy measurements [*Janssen*, 2008]. Therefore it is particularly interesting to compare wave height H_{12} derived by the CWAVE_ENV algorithm to model results and SAR measurements such as the Level 2 product introduced by ESA.

$$H_{12} = 4\sqrt{\int_{f<1/12s} S(f)\,df} \tag{17}$$

4.1 *In situ* Comparisons

Here we present the validation of SWH derived by the CWAVE_ENV algorithm against *in situ* buoy measurements over the period in December 2006, January, February and May 2007. It should be pointed out that data pairs of ASAR measurements and collocated buoys in December 2006 were not included in the tuning dataset. Buoy positions are shown in Figure 1 and listed in Table A1.

The comparison shows a reasonable agreement as given in Figure 5, and the usual statistical parameters are computed and shown as well in the Figure. One can observe that generally the empirical algorithm can provide reliable retrieved significant wave height from ASAR wave mode data with nearly zero bias, RMSE of 0.72 m and a scatter index of 24%.

To investigate the performance of CWAVE_ENV for different sea states i.e., from smooth to high sea state, a step comparison is carried out. In Table 2, the results of comparison are summarized. Besides the three statistical parameters defined in §3.2, the error percent (EP) is used as well, estimating the relative bias depending on the mean value of buoy observations:

$$EP = 100\% * (\overline{Y_i} - \overline{X_i}) / \overline{X_i} \tag{18}$$

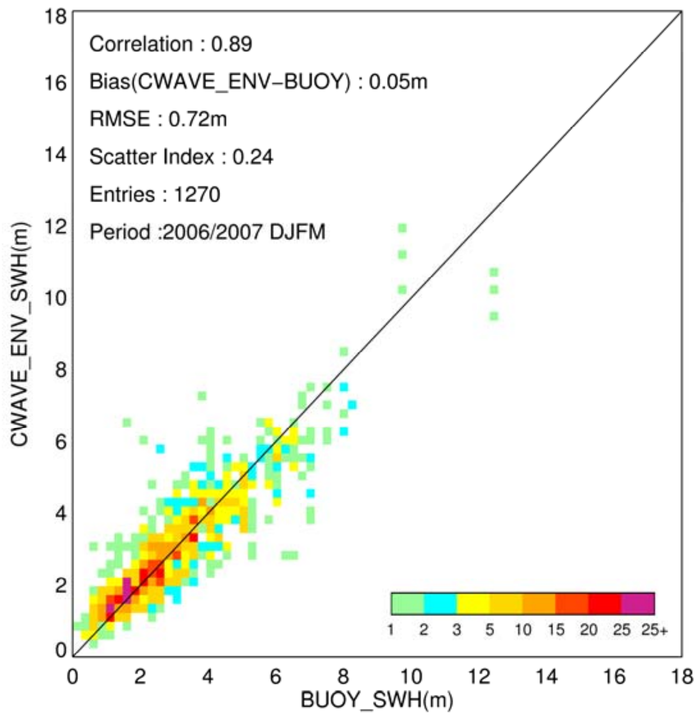

Figure 5. Scatter Plot SWH derived by the CWAVE_ENV algorithm compared to buoy in-situ measurements

Considering the usual measurement for quality, namely the scatter index, it is found that in rough sea state, i.e., SWH > 4 m, the CWAVE_ENV algorithm has a better performance with scatter indices lower than 20%. In a sea state with SWH lower than 2.5 m and particular for SWH less than 1.25 m, there is a distinct difference between CWAVE_ENV results and *in situ* observations. The error percent and scatter index in this sea state are quite large with 48.3% and 0.43 respectively. The reason might be that in the shallow water (i.e., lower than 100 m) regions, the SAR ocean wave imaging process is affected significantly by the local bathymetry while this is not resolved in the CWAVE_ENV model tuning approach using numerical wave model results.

In high sea state, namely when SWH is higher than 4m, SWH derived by CWAVE_ENV is underestimated compared to buoy measurements and the bias increases with the sea state becoming higher. However, it is interesting to note that the scatter index is lower than 15%

showing the quite promising agreement with *in situ* measurements in sea states with SWH larger than 6 m. Further investigation of the CWAVE_ENV algorithm will be considered for cases of high sea state as compared to more collocations to *in situ* measurements and to radar altimeter.

Table 2. Statistical results describing the performance of CWAVE_ENV for Hs in different sea state

SWH (m)	Data Pairs	Bias (m)	EP (100%)	RMSE (m)	SI
(0,1.25]	170	0.45	47.6%	0.60	0.43
(1.25, 2.5]	456	0.20	10.0%	0.63	0.31
(2.5,4]	370	0.07	2.0%	0.69	0.21
(4,6]	208	-0.34	7.0%	0.77	0.14
>6	66	-0.91	12.6%	1.41	0.15

4.2 Model Comparisons

In this section, SWH, H_{12} wave height and T_{m02} are compared to the ECMWF and DWD model results. More than 55, 000 data pairs are collected in January and February 2007 for the comparison. The scatter plots of Figure 6 (a) and (b) show the SWH comparisons against the ECMWF and DWD model respectively.

Both plots in Figure 6 show that SWH retrieved by the CWAVE_ENV empirical algorithm have good agreements compared to reanalysis and forecast model with zero bias, 0.43 m and 0.51m of RMSE and scatter index of 16% and 18% respectively. While for all the statistical parameters, results derived from CWAVE_ENV algorithm compared to the ECMWF reanalysis model have a better agreement than compared to the DWD model, although the differences of both comparisons are quite indistinct. A plausible explanation is that the CWAVE_ENV algorithm is tuned by the ECMWF reanalysis model. In extreme sea state, e.g., when SWH is higher than 10 m, CWAVE_ENV results have a trend lower than the ECMWF model, but higher than the DWD model. As the ECMWF model has been assimilated with the ASAR wave mode cross spectra (ESA Level1b products) using the MPI scheme, the DWD model gives a more independent comparisons.

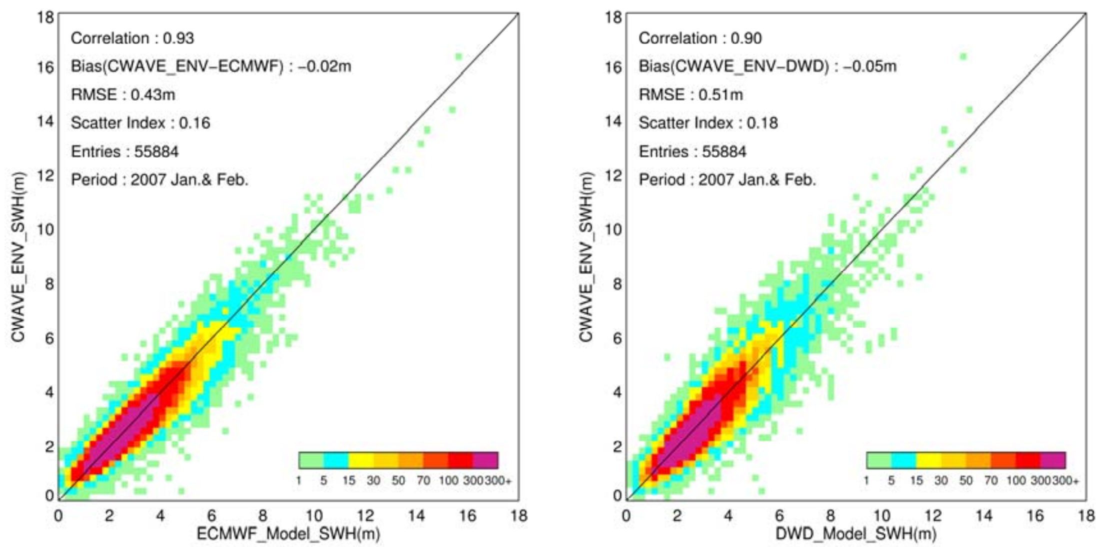

(a) (b)

Figure 6. Scatter Plot of SWH derived by CWAVE_ENV compared to the ECMWF reanalysis Model (a) and the DWD forecast model (b)

Wave height H_{12} and T_{m02} measurements are not available from the provided DWD model. Results derived from the CWAVE_ENV algorithm for these two parameters are only compared to the ECMWF reanalysis model, as shown in Figure 7 (a) and (b). Scatter index of Wave height H_{12} comparison is somehow higher to 30% while the bias still remains very low to 3 mm. T_{m02} comparison has the results for scatter index 8% and RMSE is 0.6 s.

In Table 3, statistics of three parameters derived from ASAR wave mode data as compared to model results are summarized. It is found that integral wave parameters given by CWAVE_ENV have nearly zero bias as compared to models. T_{m02} has the best scatter index of 8%, while it has the highest bias of -0.05 s and RMSE of 0.59 s in the triple comparisons.

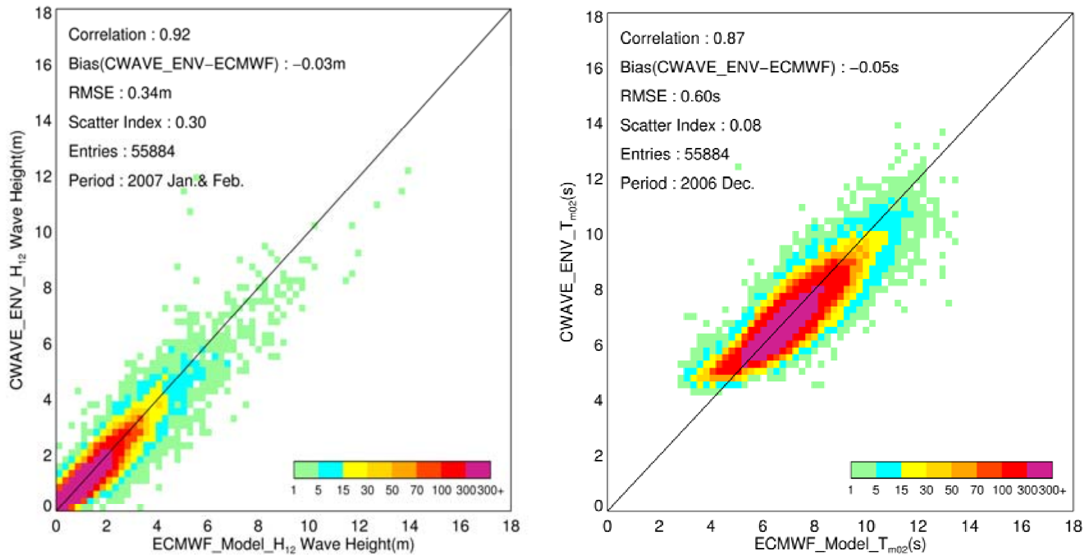

(a) (b)

Figure 7. Scatter Plot of wave height H_{12} (a) and T_{m02} (b) derived by CWAVE_ENV compared to the ECMWF reanalysis model

Table 3. Statistics obtained by the CWAVE_ENV algorithm vs. ECMWF model and DWD model for SWH (m), H_{12} wave height (m) and T_{m02} (s) in January and February 2007. Bias is with respect to observations and SI indicates scatter index.

	CWAVE_ENV vs. ECMWF model				**CWAVE_ENV vs. DWD model**			
Statistical Para.	Cor.	Bias	RMSE	SI	Cor.	Bias	RMSE	SI
SWH	0.93	-0.02m	0.43m	0.16	0.90	-0.05m	0.51m	0.18
H_{12}	0.92	-0.03m	0.34m	0.30	N/A			
T_{m02}	0.92	-0.05s	0.59s	0.08	N/A			

4.2 Compared to ESA WVW Level2 Products

In the ENVISAT mission, ESA delivers the ocean wave spectra of Level2 Products WVW to the users. The data are provided on a log-polar grid with 24 wavelengths and 36 directions. In this section, WVW products performance is compared to the result of the CWAVE_ENV algorithm for SWH and H_{12} wave height.

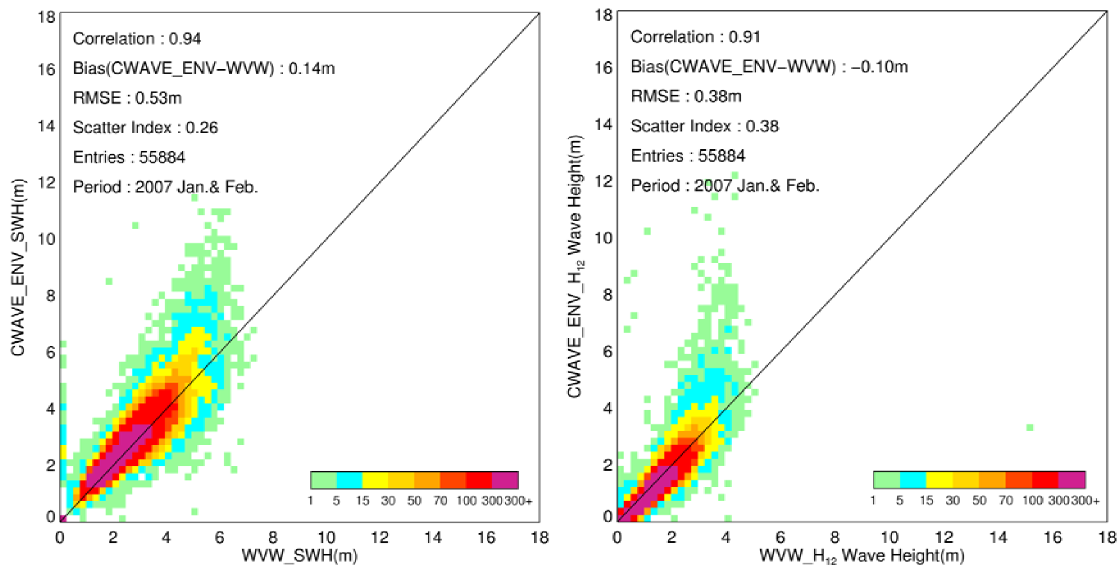

(a) (b)

Figure 8. SWH (a) and H_{12} (b) derived from ESA Level2 WVW spectra compared to CWAVE_ENV algorithm results

Figure 8 shows the two comparisons for the different wave height of SWH and H_{12} as derived from WVW products and CWAVE_ENV algorithm. One can observe that for the sea state lower than 3 m, the WVW products are generally available to provide sea state measurements, though in many cases it cannot yield the successful spectra retrieval (as shown by the original point [0,0]). When sea state is higher than 4 m, a systematic underestimation of wave height estimated from WVW products is quite obvious. It is no surprise that the algorithm is limited to retrieve long wave information contained in the SAR image.

Even if it is argued that the WVW spectra results are only available for the longer wave information resolved by the ASAR sensor, it still cannot provide reliable sea state measurements in many cases as shown for the H_{12} wave height comparison, which are in fact results for wave already longer than 220 m.

5. Global Wave Parameter Statistics

Knowledge of the global behavior climate of ocean surface waves, in terms of seasonal patterns and natural variability is of central importance to climate studies. The information used to study wave climatology comes mainly from two sources, i.e., (a) wave measurements and observations, and (b) wave models hindcast results. *In situ* measurements using wave buoys and shipborne wave recorders and visual observations from vessels participating in the Voluntary Observing Ship (VOS) scheme are the traditional data source for wave observations. Using the visual wave data along the major ship routes covering the period from 1958 to 1997, the climatology of swell and windsea in global scale is derived [*Gulev et al*., 2003].

Numerical wave models are playing an important role in wave climatology analyses. Numerous wave climatology studies, particularly regional climatology, are based on numerical wave model hindcast or reanalysis dataset, e.g., using the three wave model datasets spanning forty years, i.e., ERA-40 [*Caires and Steal*, 2003], WASA [WASA, 1993] and ODGP2 [*Wang and Swail*, 2001]. In general, all of these works show the similar wave climatology changes, e.g., compared to [*Sterl and Caires*, 2005] research, also the trend in SWH 99-percentiles of about 7 cm/year was found in North Atlantic in the study of [*Wang and Swail*, 2001]. Another point of this 40-yr's analysis of ODGP2 adds convincing support to the WASA group's conclusion that "the northeast North Atlantic has indeed roughened in recent decades, but the present intensity of the wave climate seems to be comparable with that at the beginning of this century."

Satellite remote sensing, particularly like RA and SAR, as well contributes to global wave climate analysis, although the time span still only covers about 20 years. Concentrated on the combined monthly gridded data set from ERS-1, ERS-2 and TOPEX that provides continuous coverage of the period August 1991- February 2000, the pattern with the highest variability varying in time in a similar way to the NAO was found in [*Woolf et al.*, 2002]. Using three years of reprocessed ERS-2 SAR wave mode data, global and zonal mean SWH variability is derived by [*Koenig et al.*, 2007].

In this section, global maps of mean SWH and T_{m02} derived from ASAR wave mode data are used for global integral wave parameters statistics. A dataset from December 2006, January and February 2007 is used as demonstration for a compilation of a global wave statistical analysis.

5.1 Significant Wave Height

In Figure 9 a global map of SWH retrieved by the CWAVE_ENV algorithm from ENVISAT ASAR wave mode data is shown. In some coastal regions, where the antenna stations regularly acquire data in other modes (e.g., image mode with 100 km by 100 km), wave mode data are not available, and together with the wave mode acquired in both Polar Regions, they are indicated in black color in the map.

It can be observed that in the North Atlantic and North Pacific, mean SWH is higher than in other oceanic basins. Particularly in the area between 40ºN and 60ºN and 0ºW to 50ºW region, due to seasonal storms in winter, the mean SWH is higher than 5 m.

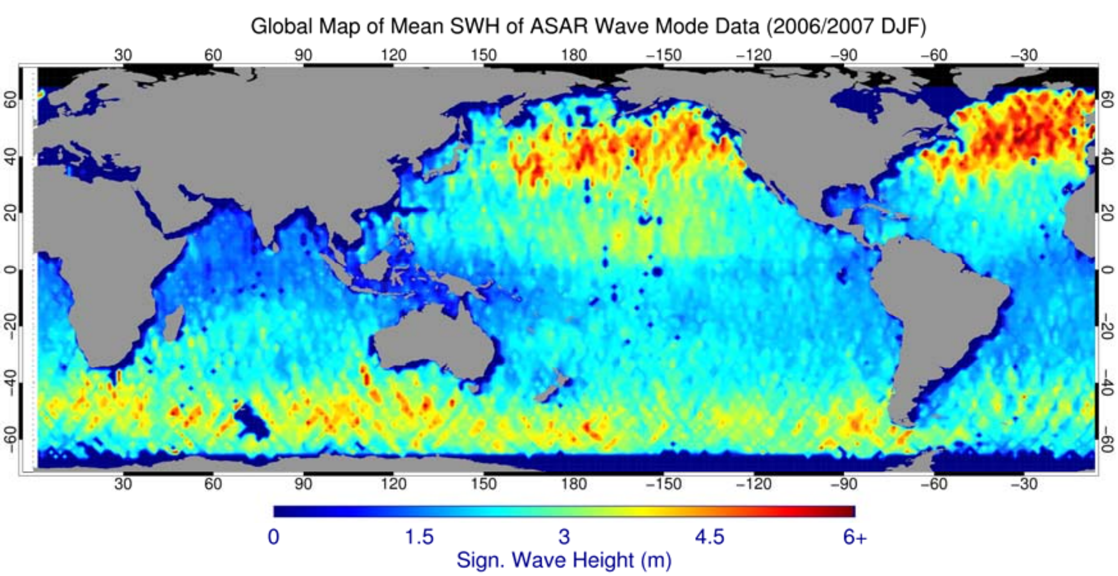

Figure 9. Mean Significant Wave Height in 1.5 by1.5 degrees boxes derived from ASAR Wave Mode Measurements

5.2 Mean Wave Period

Similar to the paragraph 5.1, a global map of mean energy wave period is compiled and shown in Figure 10. One can observe that the dominant wave period in the global ocean is around 9s. In the North Central Pacific, the distribution of wave period has approximately the same feature as the SWH shown in Figure 9. In the North Atlantic, one can observe that the high waves with average SWH higher than 5 m cover almost the entire region between 40°N to 60°N, while the wave period does not have the same feature but builds up continuousness towards the east. This shows that the North Atlantic as a fetch limited basin will steep waves towards west. High forward speed storm systems generate high waves which do not have enough space to become fully developed.

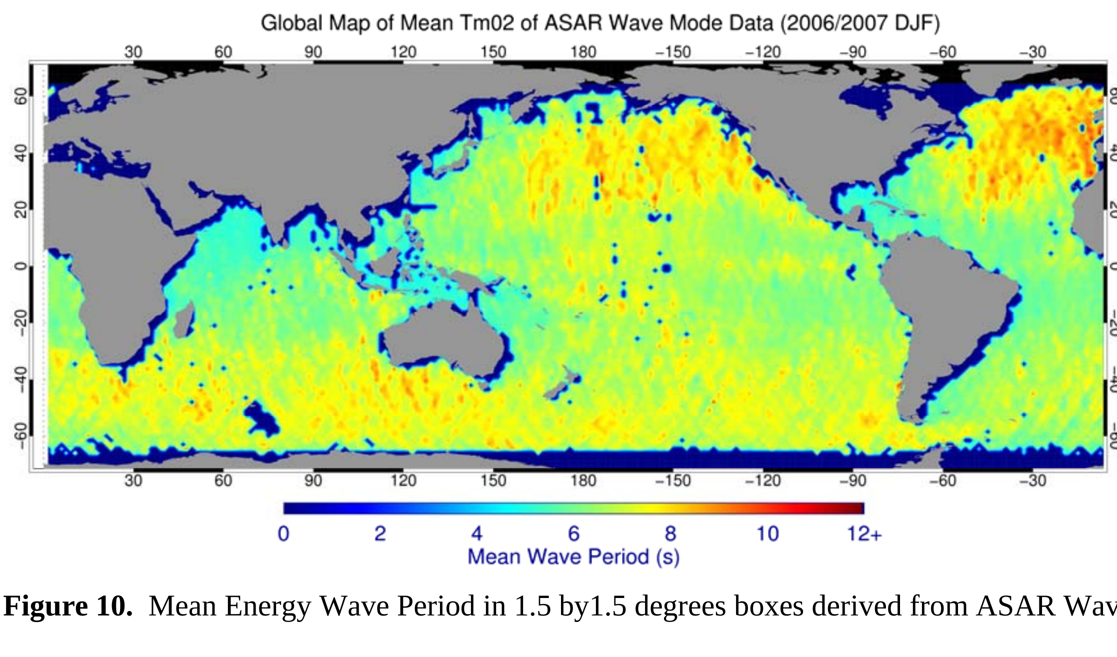

Figure 10. Mean Energy Wave Period in 1.5 by1.5 degrees boxes derived from ASAR Wave Mode Measurements

The compiled two global maps are based on three months data, which is too short to derive global wave statistical properties. Further investigation using CWAVE_ENV empirical algorithm to derive the wave statistics will be spanned the entire era of ENVISAT mission.

6. Case Studies

Two case studies are investigated in this section, a severe storm that occurred in North Atlantic on Feb. 10th, 2007 and the La Reunion extreme swell generated by a distant storm in the south. Both cases are analyzed using measurements derived from model, double tracks of ASAR and RA-2 onboard ENVISAT satellite. With respect to the storm case, performances of different SAR retrieval algorithms in extreme wind sea state are validated by model results. In the La Reunion case study, we investigate ASAR measurements over a storm which generated the high swell through the entire Indian Ocean. Based on the empirical swell propagation law, the capability of ASAR wave mode measurements used an early alarm system is analyzed as well.

6.1 North Atlantic storm event

In the section, a North Atlantic storm event is investigated in detail by satellite measurements and DWD forecast model results. In Figure 11 (a) and (c) DWD forecast model results at 0:00 and 12:00 UTC are shown in the background, on which double tracks of ASAR and RA-2 onboard ENVISAT are superimposed. ASAR provides sea surface measurements in right looking way which is around 300 km away from nadir measurements of RA-2. At 0:00 UTC, the eastern track is the ASAR and it switches to westerly at 12:00 UTC.

One can observe that there are two high wave systems moving northeasterly on Feb.10th, 2007. The eastern field showed SWH higher than 15 m given by the DWD forecast model at 0:00 UTC and made its landfall on the western coast of North Europe at about 12:00 UTC with 6 m wave height. ENVISAT acquired data are over the western high wave system twice during around 12 hours, respectively between 00:14 to 00:30 UTC acquired in the ascending pass and 12:33~12:48 UTC in the descending one.

SWH derived from satellite measurements and model forecast results through the western high wave system is further analyzed. SWH derived from ASAR using different algorithms and RA-2 along the ENVISAT tracks is represented with different colorful curves in Figure 11 (b) and (d) for 0:00 UTC and 12: 00 UTC. With respective to ASAR algorithms used for SWH measurements, CWAVE_ENV empirical algorithm is shown in blue lines, nonlinear retrieval algorithm PARSA and WVW level2 products are shown in brown and yellow one respectively. The collocated DWD forecast results with ASAR track is plotted as well with pink line.

Estimation of SWH derived from RA-2 Ku-band is used for comparison. It is represented by green lines in the plot and pink dashed lines used to denote its collocated DWD model. As RA-2 has the nadir footprints which are 300 km away with ASAR measurements, therefore the collocation measurements from is different with the ones collocated to ASAR track.

One can observe that generally the both curve plots show that SWH derived from ASAR wave mode data and RA-2 has quite well agreement with forecast model when sea state is lower than 6 m. While in the high sea state, the differences are quite distinct. At 0:00 UTC, the ASAR track is near to the high wave system yielding the higher SWH, in which PARSA algorithm provides the highest value of 11.4 m while WVW has a large underestimation only with 5.7 m. The differences of ASAR algorithms to estimate SWH in high sea state is investigated in detail.

ASAR wave mode data is acquired along the orbit every hundred kilometer as provides the sample measurements over sea surface. To avoid the high variations for SWH estimation using ASAR wave mode data in the high sea state, the averaging method is used. In the ascending pass of ENVISAT at around 0: 15 UTC, five data pairs of ASAR measurements and collocated DWD model located in the region between 42.32°N and 45.85°N which is near to the high wave system are linear averaged avoiding the effect of sampling of ASAR measurements. In the descending pass at around 12:40 UTC the area is chose as between 43.47°N to 49.63°N where eight data pairs are located with all wave heights higher than 7.0 m. The averaged SWH measurements derived from different algorithms and collocated DWD model results for both tracks are given in Table 4.

Table 4. The averaged SWH estimated from different SAR algorithms and DWD model results in higher wave field for ascending and descending pass

	CWAVE_ENV	PARSA	WVW	DWD model
Ascending Pass (at about 0:20 UTC)	8.5 m	9.6 m	5.7 m	8.4 m
Descending Pass (at about 0:20 UTC)	10.9 m	11.4 m	5.1 m	10.2 m

For the both tracks, one can observe that the CWAVE_ENV algorithm has capability to derive reliable sea state measurements even in the extreme sea state. However, the WVW products are not available to measure the high sea state. Even when the SWH is lower than 5m, it has a positive bias than other algorithms and model results, particularly obvious in the descending pass as shown with the yield line in Figure 11 (d). Therefore, from this case study, one can conclude that the WVW has a substantial under estimation in high sea state and rather high estimation in low and moderate sea state.

The PASAR algorithm in both tracks yields higher estimation than DWD model and CWAVE_ENV and moreover the positive bias increases significantly with sea state. The PARSA algorithm is implemented using the prior information from the ECMWF reanalysis model, in which the ASAR wave mode cross spectra information and RA measurements have been assimilated. Therefore, the PARSA algorithm might have an overestimation, which needs to be further validated.

At around 12:35 UTC, the RA-2 track was very near to the high wave system and yields the highest SWH estimation to be 8.9 m, which is 2.9 m higher than DWD model forecast result. In this case, performance of different SAR algorithm to derive SWH in high sea state is investigated in detail, particularly to compare the CWAVE_ENV algorithm and the existing WVW Level2 products. It is observed that the CWAVE_ENV algorithm results in both passes match the DWD model well and show reliable measurements of SWH in different sea state.

This case study gives the information that the CWAVE_ENV retrieved results are comparable to RA measurements quality and nonlinear retrieval approach while without using any prior information. Double tracks of ASAR and RA can be used jointly to validate the model performance as well for data assimilation under the condition that a suitable algorithm for SAR is adopted. In respect to the CWAVE_ENV algorithm, one issue needs to be further investigated is the performance in extreme sea state with extended dataset.

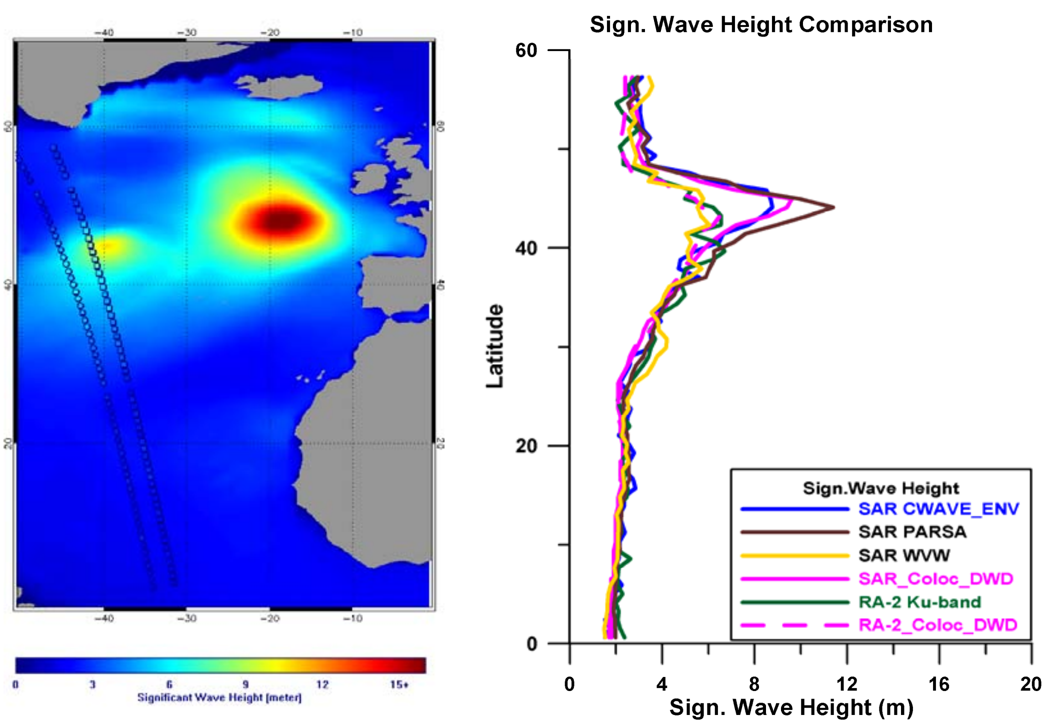

(a) (b)

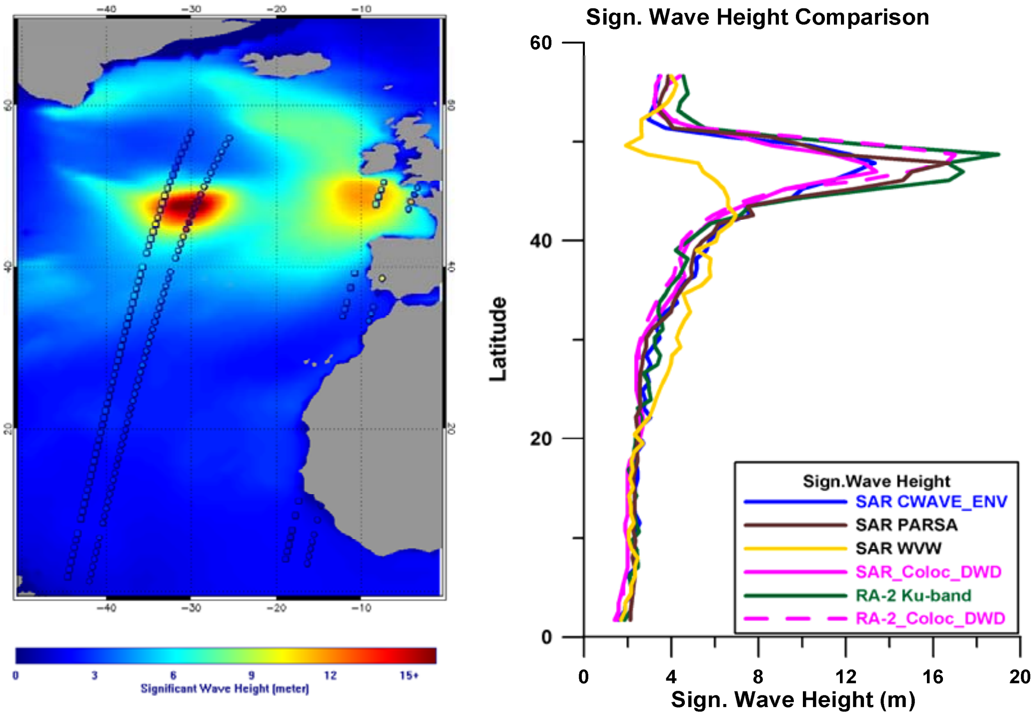

(c) (d)

Figure 11. Comparison of significant wave height derived from DWD forecast model, ASAR wave mode data and RA-2 Altimeter data for North Atlantic Storm on 10 Feb. 2007.

(a): DWD forecast model at 0:00 UTC superimposed with ASAR (eastern) and RA-2 tracks

(b) SWH derived from ASAR track using different algorithms, RA-2 and collocated DWD model results at 0: 00 UTC

(c) The same with (a) while at 12:00 UTC

(d) The same with (b) while corresponding to the tracks acquired at 12:00 UTC

6.2 Indian Ocean swells case

On the evening of May 12th, 2007, a series of very high waves broke over La Reunion Island (21°S, 55°20’E) in the Indian Ocean. The waves did numerous damages, on La Reunion and neighboring islands; several people disappeared. Those waves (i.e., extreme swell with peak period up to 19.5 s) reached on May 12 maximum heights of 11.3 m and 6.4 m of significant wave height [*Lefèvre and Aouf*, 2008].

The extreme swell is generated by a heavy storm around 40°S, South of Africa as shown in Figure12 with wind (left panel) and wave field (right panel) derived from the DWD forecast model on May 10th, 2007 at 06:00 UTC. The storm engendered swell, which propagated through the Indian Ocean covering about 1000 km/day, going over the La Reunion.

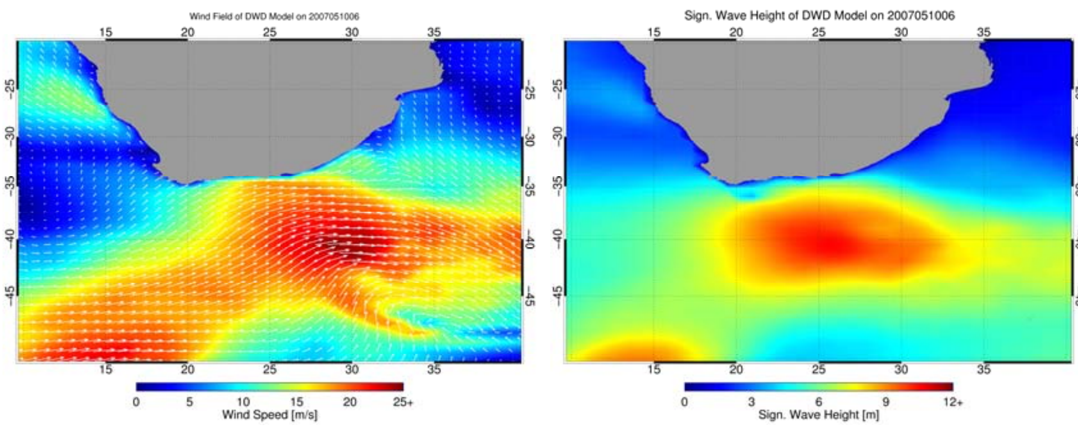

Figure 12. Wind field and SWH of DWD forecast model on 10 May, 2007 at 06:00 UTC

6.2.1 Extreme wave warning using ASAR Wave Mode data

In Figure 13, SWH measurements derived from both tracks of ASAR wave mode data using CWAVE_ENV algorithm and RA-2 data are superimposed on collocated DWD forecast model results. Time difference between the ENVISAT track and the DWD model is around 1.5 hour.

Compared to Figure12, one can observe that the storm was moving toward northeast and spanned a quite large region. At around 19:45 UTC on May 11th, the highest waves measured by ASAR wave mode track is 9.2 m located at 32.2°S, 4.7°E. It can be identified that higher wave trains traveled to the northeast and arrived at La Reunion Island on May 12th at around 16 UTC after traveling 1700~2000 km. With straightforward wave propagation relationships against traveling distance introduced in [*Dietrich et al.*, 1975], about 5 m waves can be forecasted in Reunion Island at around 12:00~16:00 UTC on May 12th. This shows good agreement with in situ and reanalysis model, which yields 6 m [*Lefèvre and Aouf*, 2008].

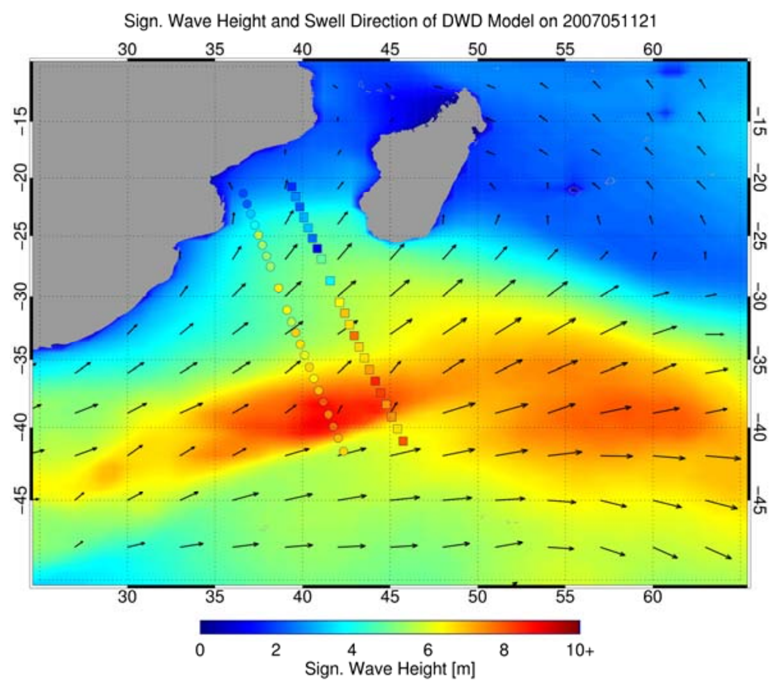

Figure 13. Significant wave height and swell direction of DWD model on May 11th, 2007 at 21:00 UTC. Double tracks of ASAR wave mode (squares) and RA-2 (circles) at around 19:45 UTC are superimposed.

In this case, around 20 hours earlier the extreme swell arriving at Reunion Island can be forecasted by ASAR wave mode measurements derived from the CWAVE_ENV algorithm. The ASAR wave mode data also might be used as an extreme wave forecast tool. Together with the numerical forecast model, both can be used to validate each other and thus an extreme wave early warning system is possible.

7 Conclusions

An empirical approach referred to as CWAVE_ENV to estimate integral wave parameters from ASAR wave mode data without first guess information is presented in this paper. The empirical model function is tuned using globally distributed ASAR wave mode data and collocated ECMWF reanalysis model spectra. The tuning approach is implemented with stepwise regression method to select ASAR image parameters and the model parametric coefficients are derived by cost function minimization.

Validation of the CWAVE_ENV algorithm is carried out by comparison against *in situ* buoys measurements, numerical wave model and ENVSIAT/ASAR WVW Level 2 products. Brief summary of the algorithm validation are given in following.

(1) SWH retrieved from ASAR data compared to buoy *in situ* measurements show good correlation of 0.9, reasonable RMSE of 0.73 m and 0.25 for SI. Investigating the comparison of CWAVE_ENV algorithm in different sea state demonstrates that the algorithm has better performance in rough sea state (with SWH higher than 4.0 m) than for SWH less than 2.5 m.

(2) The performance for SWH, H_{12} wave height and T_{m02} compared to the ECMWF reanalysis models is presented. In respect to the wave height (SWH and H_{12}) comparisons, CWAVE_ENV results have a low bias of -0.02 m and -0.03 m and RMSE of 0.43 m and 0.34 respectively, while the wave period comparison shows the lowest SI of 8%.

As the SAR independent dataset when compared to ECMWF reanalysis model, the DWD model compared to the CWAVE_ENV algorithm results therefore show more realistic results. Comparison results show that SWH derived by the CWAVE_ENV algorithm has a small negative bias of 0.05 m and SI of 18%.

(3) CWAVE_ENV retrieved results of SWH and H_{12} are also compared to the ENVISAT ASAR wave mode Level2 products. The comparison results reveal that the existing Level2 products strongly underestimate SWH and the measurements vary with the change of ASAR cut-off wavelength.

Case studies:

The results of the two case studies show that the CWAVE_ENV algorithm performs well, even in extreme sea state.

In the North Atlantic storm event case study, SWH given by the double tracks of ASAR and RA-2 are compared to the DWD forecast model. All measurements derived from radar and models agree each other well along the orbit, but in the extreme high sea state in the storm there are distinct differences. CWAVE_ENV results agree well with DWD being around a half meter higher for sea state higher than 7 m. Both RA-2 and ASAR PARSA results are higher than SWH given by the model with bias more than 1 m in this extreme sea state. The ASAR level 2 products WVW show significant underestimation of wave height in the area of high wave systems.

The analysis of the La Reunion case demonstrated that ASAR wave mode data can be used as forecasting tool for extreme waves when using the wave retrieval algorithm CWAVE_ENV. It might alternate another approach to construct a global extreme warning system.

In spite of the overall good quality of integral wave parameters derived by CWAVE_ENV algorithm, the assessment is based on the dataset in three months period. Therefore more investigations are needed by collecting *in situ* buoy measurements, cross over RA measurements to confirm its performance in high extreme sea state for further improvements. The algorithm will be implemented into the whole ENVISAT era since 2002 in the near future for validation and global sea state statistics.

Appendix A: List of Buoys Used for CWAVE_ENV Algorithm Validation

Name, latitude and longitude of buoys used for CWAVE_ENV empirical algorithm validation is given in Tab. A1. The positions of the buoys are shown in Fig. 2 in §2.3.

Table A1. Name, Latitude and Longitude of buoys used for validation, corresponding to the red cross marks shown in Fig. 2

Station	Latitude	Longitude	Station	Latitude	Longitude
NODC_41001	34°44'N	72°41'W	**NODC_51001**	23°26'N	162°13'W
NODC_41002	32°19'N	75°22'W	**NODC_51002**	17°11'N	157°47'W
NODC_41009	28°30'N	80°10'W	**NODC_51003**	19°13'N	160°49'W
NODC_41010	28°57'N	78°29'W	**NODC_51004**	17°31'N	152°29'W
NODC_42001	25°54'N	89°40'W	**NODC_51028**	0°01'S	153°52'W
NODC_42002	25°10'N	94°25'W	**NODC_fpsn7**	33°29'N	77°35'W
NODC_42003	26°04'N	85°56'W	**NODC_46063**	34°16'N	120°42'W
NODC_42019	27°55'N	95°22'W	**NODC_46066**	52°42'N	154°59'W
NODC_42020	26°56'N	96°42'W	**NODC_46084**	56°35'N	136°10'W
NODC_42035	29°14'N	94°25'W	**MEDS_C44137**	42°17'N	62°00'W
NODC_42036	28°30'N	84°31'W	**MEDS_C44140**	43°45'N	51°45'W
NODC_42039	28°47'N	86°01'W	**MEDS_C44141**	43°00'N	58°00'W
NODC_42040	29°11'N	88°13'W	**MEDS_C44251**	46°26'N	53°23'W
NODC_44004	38°29'N	70°26'W	**MEDS_C44255**	47°17'N	57°21'W
NODC_44008	40°30'N	69°26'W	**MEDS_C44258**	44°30'N	63°24'W
NODC_44011	41°07'N	66°35'W	**MEDS_C46004**	50°56'N	136°05'W
NODC_44014	36°37'N	74°50'W	**MEDS_C46036**	48°21'N	133°56'W
NODC_44025	40°15'N	73°10'W	**MEDS_C46131**	49°55'N	124°59'W
NODC_46002	42°36'N	130°16'W	**MEDS_C46132**	49°44'N	127°56'W
NODC_46005	46°01'N	130°58'W	**MEDS_C46134**	48°40'N	123°29'W
NODC_46011	34°53'N	120°52'W	**MEDS_C46145**	54°22'N	132°25'W
NODC_46012	37°22'N	122°53'W	**MEDS_C46146**	49°20'N	123°44'W
NODC_46013	38°14'N	123°19'W	**MEDS_C46183**	53°37'N	131°06'W
NODC_46014	39°12'N	123°58'W	**MEDS_C46184**	53°55'N	138°51'W
NODC_46015	42°45'N	124°51'W	**MEDS_C46185**	52°25'N	129°49'W
NODC_46022	40°47'N	124°32'W	**MEDS_C46204**	51°22'N	128°45'W
NODC_46023	34°42'N	120°58'W	**MEDS_C46205**	54°10'N	134°17'W
NODC_46025	33°45'N	119°05'W	**MEDS_C46206**	48°50'	126°00'W
NODC_46027	41°51'N	124°23'W	**MEDS_C46207**	50°53'N	129°55'W
NODC_46028	35°44'N	121°53'W	**MEDS_C46208**	52°31'N	132°41'W
NODC_46029	46°08'N	124°31'W	**EUROP_41100**	15°54'N	57°54'W
NODC_46035	57°03'N	177°35'W	**EUROP_41101**	14°36'N	56°12'W
NODC_46042	36°45'N	122°25'W	**EUROP_62001**	45°12'N	5°00'W
NODC_46047	32°26'N	119°32'W	**EUROP_62029**	48°42'N	12°30'W
NODC_46050	44°38'N	124°30'W	**EUROP_62081**	51°00'N	13°24'W
NODC_46053	34°14'N	119°52'W	**EUROP_62105**	55°24'N	12°24'W
NODC_46059	38°02'N	130°00'W	**EUROP_62108**	53°30'N	19°24'W
NODC_46061	60°14'N	146°50'W	**EUROP_62163**	47°30'N	8°24'W
			EUROP_64045	59°06'N	11°42'W

Appendix B: SAR Image Spectrum Estimation Using Periodogram Method

A two-dimensional ASAR image with the size of B_x and B_y size in range and azimuth direction are divided into nb_x and nb_y subscenes respectively. The relation is given by,

$$nb_x = B_x / n_x \ , \ nb_y = B_y / n_y \qquad \text{(B1)}$$

Where n_x =256 and n_y =512 are taken to be the subscene size used to divide the entire samples of B_x and B_y in range and azimuth direction. The two-dimensional FFT is performed on every subscene, i.e., normalized subscene G (computed via (8)) with pixel size n_x and n_y.

$$F_G = fft_{nx*ny}(G) \qquad \text{(B2)}$$

The power density spectrum for every subscene denoted by P_S,

$$P_S = (F_G)^2 \qquad \text{(B3)}$$

Summing the subscenes power density spectrum and averaging to reduce the variance, the entire ASAR image spectrum P is given by (12),

$$P = \frac{1}{nb_x * nb_y} \sum P_S \qquad \text{(B4)}$$

The Fourier transform theory states that the integral of the image in the frequency domain equals to the image variance in the spatial domain. The Cartesian spectrum computed in step (12) needs to be normalized to ensure this case. The normalized ASAR image spectrum is denoted as $\overline{P}$,

$$\overline{P} = P * \left(\sum P * dk_x * dk_y \right)^{-1} \qquad \text{(B5)}$$

In (13) dk_x, dk_y is the wave number spacing in ASAR image range and azimuth direction, given by,

$$dk_x = 2\pi / (B_x * d_x) \quad , \ dk_y = 2\pi / (B_y * d_y) \qquad \text{(B6)}$$

d_x, d_y is the pixel spacing in meters of ASAR image.

The ASAR parameters to be used for the CWAVE_ENV model are then computed from the SAR image spectrum $\overline{P}$ by projection onto the subspace spanned by the orthonormal functions, i.e., by computing the respective scalar products.

$$S = \sum \overline{P}\left(k_x, k_y\right) h_i(k_x, k_y) dk_x dk_y \qquad \text{(B7)}$$

where $1 \le i \le n_\varphi n_k$ and h_i is the orthonormal functions and their exact forms are proposed in the CWAVE_ENV model.

8 References

Abdalla, S., P. A. E. M. Janssen and J.-R. Bidlod (2008), Status of global validation of ENVISAT ASAR Wave Mode Products at ECMWF, in Proc. SEASAR workshop, ESRIN, Frascati, Italy, 2008, ESA-SP656.

Alpers, W and C. Brüning (1986), On the relative importance of motion-related contributions to the SAR imaging mechanism of ocean surface waves, *IEEE Trans. Geosci., and Rem. Sens.*, 24, 873-885.

Beal, R.C., D.G. Tilley, and F.M. Monaldo (1983), Large- and small-scale spatial evolution of digitally processed ocean surface wave spectra from the Seasat synthetic aperture radar, *J. Geophys. Res.*, 88, 1761-1778.

Behrens, A. and H. Günther (2008), Operational wave prediction of extreme storms in Northern Europe, Natural Hazards, doi: 10.1007/s11069-008-9298-3, 2008.

Bidlot, J.-R., J.-G. Li, P.Wittmann, M. Fauchon, H.-S. Chen, J.-M. Lefèvre, Th. Bruns, D. Greenslade, F. Ardhuin, N. Kohno, S. Park and M. Gomez (2007), Inter-comparison of operational wave forecasting systems, paper presented at 10th International workshop on wave hindcasting and forecasting and coastal hazard symposium, OAHU, Hawaii, November 11 – 16, 2007.

Caires, S. and A. Sterl (2003), Validation of ocean wind and wave data using triple collocation, *J. Geophys. Res.*, vol.108 (C3), doi: 10.1029/2002JC001491.

CERSAT – IFREMER, (2002), Envisat ASAR Wave Mode collocated products, version 1.6, XCOL-MUT-S-02-IF, Brest, France.

Dietrich, G., Kalle, K. W. Krauss and G. Siedler (1975), Allgemeine Meereskunde. Eine Einfruehrung in die Ozeanographie, Gebrueder Borntraeger, Berlin.

Engen, G. and H. Johnson (1995), SAR-ocean wave inversion using image cross spectra, *IEEE Trans. Geosci., and Rem. Sens.*, 33, 329-360.

European Space Agency (2007), *ENVISAT ASAR Product Handbook*, Issue 2.2.

G. Brooker (1995), UWA processing algorithm specification, version 2.0,Tech. Rep., ESA, ESTEC/NWP, Noordwijk, The Netherlands.

Gulev, S. K., V. Grigorieva, A. Sterl, and D. Woolf (2003), Assessment of the reliability of wave observations from voluntary observing ships: Insights from the validation of a global wind wave climatology based on voluntary observing ship data, *J. Geophys. Res.*, 108(C7), 3236, doi:10.1029/2002JC001437.

Günther, H., S. Hasselmann, and P.A.E.M., Janssen (1992), The WAModel cycle 4 (revised version), Technical report, Deutsches Klimarechenzentrum (DKRZ), Hamburg, Germany, 1992.

Hasselmann, K. and S. Hasselmann (1991), On the nonlinear mapping of an ocean wave spectrum into a synthetic aperture radar image spectrum, *J. Geophys. Res.*, 96, 10713-10729.

Hasselmann, K., R.K. Raney, W. J. Plant, and et al., (1985), Theory of synthetic aperture radar ocean imaging: A MARSEN view, *J. Geophys. Res.*, 90, 4659-4686.

Heimbach, P., S. Hasselmann, and K. Hasselmann (1998), Statistical analysis and intercomparison with WAM model data of three years of global ERS-1 SAR wave Mode Spectral retrievals, *J. Geophys. Res.*, 103, 7931–7977.

Janssen, P. A. E. M. (2008), Progress in ocean wave forecasting, *J. Comput. Phys.*, 227, 3572-3594.

Kerbaol, V., B. Chapron, and P. W. Vachon (1998), Analysis of ERS-1/2 synthetic aperture radar wave mode imagettes, *J. Geophys. Res.*, 103, 7833–7846.

König, Th., S. Lehner, and J. Schulz-Stellenfleth (2007), Global analysis of a 2 year ERS-2 wave mode dataset over the Ocean, in Proc. of IGARSS 2007, Barcelona, Spain.

Krogstad H.E. (1992), A simple derivation of Hasselmann's nonlinear ocean –synthetic aperture radar transforms, *J. Geophys. Res.*, 97(C2), 2421-2425.

Lefèvre, J.-M. and L. Aouf (2007), Use of wind/wave satellite data for numerical wave predictions at Meteo-France, Presented paper in Globe Wave workshop, Brest 19-21 September 2007.

Lehner, S., J. Horstmann and W. Koch (1998), Mesoscale wind measurements using recalibrated ERS SAR images, *J. Geophys. Res.*, 103, 7847-7856.

Lehner, S., J. Schulz-Stellenfleth, J. B. Schättler, H. Breit, and J. Horstmann (2000), Wind and wave measurements using complex ERS-2 wave mode data, *IEEE Trans. Geosci., and Rem. Sens.*, 38, 2246-2257.

Li, X.-M., S. Lehner and M.-X. HE (2008), Ocean wave measurements based on satellite synthetic aperture radar (SAR) and numerical wave model (WAM) data - extreme sea state and cross sea analysis, *Int. J. Remote Sensing*, 29 (21), 6403 - 6416, doi: 10.1080/01431160802175546.

Mastenbroed, C. and C. de Valk (1998), A semi-parametric algorithm to retrieve ocean wave spectra from synthetic aperture radar, *J. Geophys. Res.*, 105, 3497-3516.

Schulz-Stellenfleth, J., S. Lehner, and D. Hoja (2005), A parametric scheme for the retrieval of two-dimensional ocean wave spectra from synthetic aperture radar look cross spectra, *J. Geophys. Res.*, 110, doi: 10.1029/2004JC002822.

Schulz-Stellenfleth, J., Th. König and S. Lehner, (2007), An empirical approach for the retrieval of integral ocean wave parameters from synthetic aperture radar data, *J. Geophys. Res.*, 112, doi: 10.1029/2006JC003970, 2007.

Steele, K.E., and M.D. Earle (1979), The status of data produced by NDBC Wave Data Analyzer (WDA) system, in *Proc.* Oceans'79, San Diego, CA, Marine Technology Society and IEEE, 212-220.

Sterl, A. and S. Caires (2005), Climatology, Variability and Extrema of Ocean Waves - The Web-based KNMI/ERA-40 Wave Atlas, *Int. J. Climatology*, 25(7), 963-997, doi:10.1029/joc.1175.

Stoffelen, A., and D. Anderson (1997), Scatterometer data interpretation: Estimation and validation of the transfer function CMOD4, *J. Geophys. Res.*, 102, 5767– 5780.

von Storch, H. and F. Zwiers (1999), Statistical Analysis in Climate Research, Cambridge Univ. Press, NewYork.

WAMDI GROUP (1998), The WAM model a third generation ocean wave prediction model, *J. Phys. Oceanogry.*, 18, 1775-1810.

Wang, X.L., and V.R. Swail (2001), Changes of extreme wave heights in northern hemisphere oceans and related atmospheric circulation regimes, *J. Climate*, 14, 2204-2221, 2001.

WASA (1998), Changing waves and storms in the Northeast Atlantic? *Bull. Amer. Met. Soc.*, 79, 741-760.

Weisse, R., H. von Storch, and F. Feser (2005), Northeast Atlantic and North Sea Storminess as Simulated by a Regional Climate Model during 1958–2001 and Comparison with Observations, *J. Climate*, 18, 465–479.

Woolf, D.K., P.G. Challenor, and P.D. Cotton (2002), Variability and Predictability of the North Atlantic wave climate, *J. Geophys. Res.*, 107, 3145-3158, doi:10,1029/2001JC001124.